Experiments in Fluids 17 (1994) 1–9 © Springer-Verlag 1994

An experimental study of receptivity of acoustic waves in laminar boundary layers

M. D. Zhou, D. P. Liu, R. F. Blackwelder

Abstract The receptivity of a laminar boundary layer developing on a flat plate was studied with two- and three-dimensional roughness elements. The layer was subjected to acoustic waves from speakers orientated perpendicular to the surface of the plate. Visualization of the transition patterns were obtained by heating temperature sensitive liquid crystals on the plate and observing the cooling patterns associated with the different flow regimes. Hot-wire data showed that the most amplified Tollmien–Schlichting waves dominated the downstream growth when the roughnesses were placed within the linearly unstable regime. The receptivity depended upon the size and aspect ratio of the three-dimensional roughness as predicted by Choudhari and Kerschen 1990.

List of Symbols

D	diameter of roughness
δ	boundary layer thickness
Δx	streamwise spatial separation
Δz	spanwise spatial separation
ε	$(Re)^{-1/8}$
f	frequency
h	nondimensional roughness height, $H/(\varepsilon^5 L)$
H	height of roughness
H^*	nondimensional roughness height, H/δ
l_x	streamwise length of roughness
l_z	spanwise length of roughness
L	distance of the roughness element from leading edge
λ	wavelength of Tollmien–Schlichting wave
ν	kinematic viscosity coefficient
Re	Reynolds number, $U_\infty L/\nu$
R_{uu}	Correlation coefficient
SPL	sound pressure level
SPL*	SPL normalized by 124 dB
θ	angle between speaker and roughness
τ	time delay
u	streamwise velocity
U_∞	freestream velocity
W	width of two-dimensional roughness
x	distance from leading edge
y	distance normal to the wall
z	spanwise coordinate

Subscripts

$(\ )_{ac}$	acoustic
$(\ )_r$	roughness
$(\ )_m$	measurement location

1 Introduction

It is well known that the performance of aircraft, heat exchangers, pipe lines, etc. strongly depend on the characteristics of the turbulent wall layer. And in turn, the latter depends strongly on the laminar-turbulence transition process which is quite sensitive to the environmental disturbances even at small amplitudes. Generally boundary layer transition may be regarded as the forced response of a very complicated oscillator, i.e. the laminar boundary layer, to an external disturbance. This response can be divided into several stages: receptivity, linear instability and amplification, secondary instability, nonlinear amplification, and breakdown. The first stage, receptivity, concerns the processes by which the available environmental disturbances initially generate a linear instability in the shear layer. In the past, most of the research effort has been directed towards understanding the linear instability mechanisms and the following stages of transition. However experiments in different facilities have often produced different results leading to an effort during the past few years to understand how the initial disturbances are initiated into the boundary layer. The study of receptivity has become a key element in the study of predicting and controlling transition.

Unfortunately, receptivity is more complicated than linear amplification and nonlinear breakdown because it can involve many different environmental disturbances and input mechanisms. In addition, our knowledge of receptivity is limited because it has only been the object of intense study during the past decade. The first rigorous study of receptivity of disturbances near the leading edge was due to Goldstein 1983. His theory examined the production of Tollmien–Schlichting waves due to sound interacting with the laminary boundary layer in a region where the mean flow changes rapidly in the streamwise direction. Depending upon the geometry, the instability waves generated by this type of receptivity often

Received: 5 August 1992/Accepted: 6 February 1993

M. D. Zhou, D. P. Liu, R. F. Blackwelder
Department of Aerospace Engineering, University of Southern California, Los Angeles, CA 90089-1191, USA

Correspondence to: R. F. Blackwelder

This research was partially funded by the Office of Naval Research under Contract N00014-89-J-1400. Their support is gratefully acknowledged. We also thank one of the reviewers for his helpful comments.

undergo substantial decay before they reach the unstable amplification region of the boundary layer. Goldstein 1985 and Kerschen, Choudhari and Heinrich 1989 have analyzed receptivity which occurs when acoustic waves interact with a two dimensional roughness or a porous surface. Nishioka and Morkovin 1986, and Kerschen 1989 and 1990 further developed the theoretical understanding of this type of the receptivity.

Following this concept, Choudhari and Kerschen 1990 analyzed the corresponding receptivity problem with a three dimensional roughness element. Their results showed that the acoustic wave orientation and the details of the geometry of the wall inhomogeneity, i.e. the roughness element, have a significant influence on the generation of the instability waves. Although these theoretical results have been quite encouraging, they are all limited to small perturbations.

On the experimental side, Nishioka and Morkovin 1986 used a three dimensional sound source interacting with a two dimensional boundary layer. Their source was placed approximately one wave length above their smooth flat plate in an example of what Kerschen 1989 called "forced receptivity". Recently Saric, Hoos and Radeztsky 1991 performed an experimental study with acoustic excitation generated by a loudspeaker located far upstream of the leading edge. They studied the interaction of the acoustic disturbance with a two dimensional roughness and measured some of the parametric influences such as thickness.

The present research was undertaken to investigate the influences of additional parameters on the receptivity process, including different geometries for the two dimensional roughness and the first use of isolated three dimensional roughness elements. In addition, the acoustic excitation was introduced downstream of the leading edge. This allowed the effects of the interaction of acoustic waves with the roughness elements to be studied more directly without any strong contamination due to the receptivity from the leading edge. The acoustical source of the contamination waves was many Tollmien–Schlichting wavelengths from the roughness so that 'natural receptivity' was explored. This differs from the 'forced receptivity' of Nishioka and Morkovin 1986 whose disturbance was much closer to the plate (see Kerschen 1989). The limitations of the linear theory were also sought. Some of the principal theoretical background is given in the appendix for comparison.

2
Experimental conditions

2.1
The main facility

The experiments were performed in the 60 cm × 90 cm Low Turbulence Wind Tunnel at the University of Southern California described by Blackwelder and Haritonidis 1983. The free stream turbulence level was 0.03–0.04% over the velocity range of 5–17 m/s. The experiments were performed on a 0.9 m × 6 m smooth flat plate 6.4 mm thick sketched in Fig. 1. It had a 9:1 (major/minor) elliptical leading edge which provided a well controlled initiation point for the laminar boundary layer. A trailing edge flap and screens at the trailing edge of the flat plate shown in Fig. 1 were used to control the location of the stagnation point. A microphone was flush mounted on the centerline of the plate 60 cm from the leading

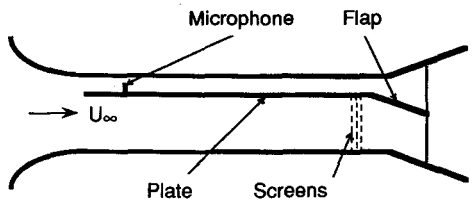

Fig. 1. The test section and the flat plate

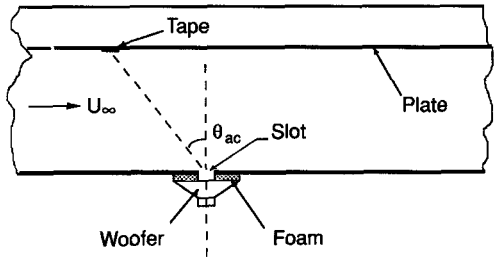

Fig. 2. The excitation system

edge to monitor the amplitude of the acoustical disturbances. A global check on the flow quality showed that the Reynolds number corresponding to the first occurrence of the turbulent spots was about $U_\infty x/\nu \approx 2.3 \times 10^6$.

Plastic tapes with various plan forms and thicknesses were fixed at chosen locations on the plate to form the required roughness. The excitation system (Fig. 2) consisted of two 50 watt 20 cm woofers located at the same streamwise location. They were driven in parallel by a function generator-amplifier system. To minimize the contamination due to leading edge receptivity, the acoustic waves were beamed from the side wall of the test section located 0.5 m from the test plate as illustrated in Fig. 2. To insure that the speakers did not cause any mechanical vibrations of the experimental system, they were mounted on an independent stand, external to the tunnel. Their acoustical disturbance was beamed through a spanwise slot in the tunnel wall opposite the test plate. The slot could be positioned over a wide range of streamwise locations with respect to the tape so that the angle θ_{ac} could be varied. The gap between the woofers and the tunnel was filled with the plastic foam to minimize the flow disturbance. A right handed Cartesian coordinate system with x, y, and z in the streamwise, normal and the spanwise direction was used.

2.2
Hot-wire measurements

Single hot-wire probes were used to measure the velocity fluctuations. The speaker's forcing signal and the hot-wire signals were simultaneously acquired by an analog-to-digital converter so that linearization, phase averaging, spectra, correlation etc. could be processed by an IBM PC AT-386 computer as required. The fixed quarter inch microphone was used to measure the reference signal and to set the excitation intensity. It was calibrated against a one inch microphone at the roughness location when the wind tunnel was not running.

To facilitate this study of receptivity, the following conditions were imposed and followed throughout the experiments. First the y location of the hot wire probe, i.e. its distance normal to

the wall, was always kept at the critical layer of the boundary layer (approximately $0.2\,\delta$) to maximize the signal response. Secondly the initial Tollmien–Schlichting instability waves were often too small to measure accurately. Thus a fetch distance between the roughness and the hot-wire probe was necessary to allow for sufficient growth. The fetch distance was chosen to be 0.6–1.0 m to minimize the influence of nonlinear amplification of the disturbances on the measurements. Thirdly, the linearized hot-wire signals were always phase averaged with respect to the acoustical signal. This standard procedure averaged over typically several hundred cycles at the frequencies used in this study. Fourthly, with the three-dimensional roughness elements, the spanwise location of the measurements becomes an issue. A typical spanwise distribution of the flow response with an artificial roughness is shown in Fig. 3. The hot-wire probe was always stationed at the spanwise location of the center of the measured roughness disturbance throughout, i.e. $z \approx 0$. Lastly, the hot-wire signal recorded during the interaction of an acoustic wave with a roughness element usually include not only the *T–S* instability waves but also the remnant influence of the leading edge receptivity, the influence of the background roughness of the plate, the Stokes waves and any remaining vibration caused by the excitation system. Corrections for these effects were obtained experimentally by conducting a background experiment without the roughness element. These signals were phase averaged to obtain the educted base flow conditions. After the roughness element was added and the experiment repeated, the educted base flow results were subtracted from the phase averaged signals with the roughness.

For typical experimental conditions, the streamwise location of the roughness, L, was 1.15 m and the hot-wire probe, x_m, was at 1.8 m. With a free stream velocity of 13 m/sec, these conditions corresponded to Re_L of 1×10^6 and Re_x of 1.6×10^6 respectively. The differing roughness thicknesses were always within the range $0.01 < H^* < 0.08$ when compared with the boundary layer thickness and within $0.21 < h < 2.6$ using the lower deck of the triple deck theory for comparison. The excitation frequency was typically 74 Hz and the intensity was 97 db. The actual experimental conditions are given with each figure.

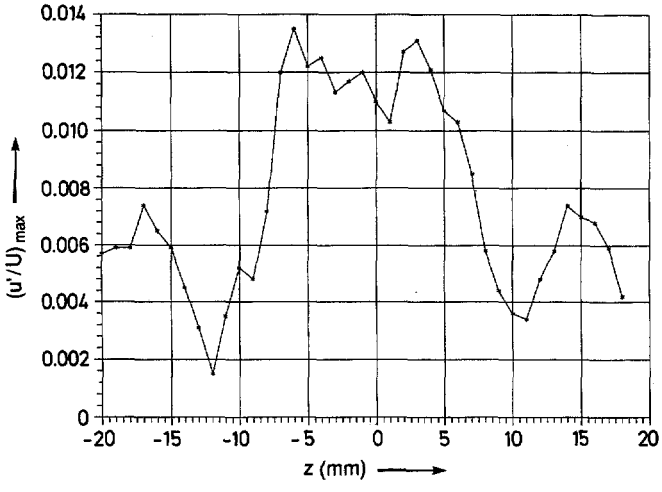

Fig. 3. Spanwise amplitude distribution of the phase averaged streamwise velocity amplitude for $H = 0.375$ mm and $x_m = 1.8$ m

2.3
Liquid Crystal Flow Visualization

The flow was visualized by two different techniques; temperature sensitive liquid crystals were spray painted onto the plate and commercially available sheets of liquid crystals were used. Both were produced by Hallcrest Co. and could be ordered in temperature ranges of 30–35, 33–37 and 35–40 °C. The sheets had an area of 30 cm × 30 cm and were 0.25 mm thick. When heated, the liquid crystals changed color progressively from black at the low temperature to red, yellow, green and blue as the temperature increased within the temperature ranges stated above. The time constants of the liquid crystals depends upon the heat capacity of the crystals. The thin spray painted layer responded with a time constant of typically 5 s and the thicker sheet had a time constant of typically 20 s.

An experimental run usually was conducted as follows; all of the experimental conditions were established including the freestream velocity but with no acoustic disturbance. The liquid crystals were heated by infrared lamps until the whole test area was uniformly blue; then the acoustical excitation was turned on. The liquid crystals were cooled at different rates according to the nature of the flow; for example, steady vortical flows offered the highest rate of heat transfer, followed by turbulent flows. Laminar flow regimes produced the minimum heat transfer. In this manner, different flow regions could be distinguished by viewing the different color patterns. To check the operational mode of the liquid crystals, a preliminary test was conducted with a 28 mm diameter circular cylinder shown in Fig. 4. The well known necklace vortex is clearly indicated. An induced pair of vortices in the spanwise region are seen approximately 10 diameters downstream.

Figure 5 shows a set of photographs for the three-dimensional roughness. Except for the acoustic forcing amplitude, the flow conditions are the same for all four photographs. The signals from the hot-wire sensor in the photos are shown in the lower left hand corner so that a comparison with the liquid crystal patterns is obtained. As the excitation level increased gradually (see caption), a continuous change of the color occurred corresponding to the transition sequence from the laminar region to the turbulent one. At the maximum excitation in Fig. 5d, the sound level was 97 db at the roughness.

3
Results and discussions

3.1
The mechanisms of receptivity

To investigate the main mechanism of receptivity, hot-wire measurements were carried out for four flows, i.e. (a) the background flow with no external excitation and no artificial roughness; (b) flows with artificial roughness but with no excitation; (c) flows with excitation but with no artificial roughness; and (d) flows with both artificial roughness and excitation. The phase averaged signals and the spectra for these four flow conditions are shown in Fig. 6 and 7. For these figures the Reynolds number based on the streamwise distance of the roughness from the leading edge was 0.28×10^6. The hotwire

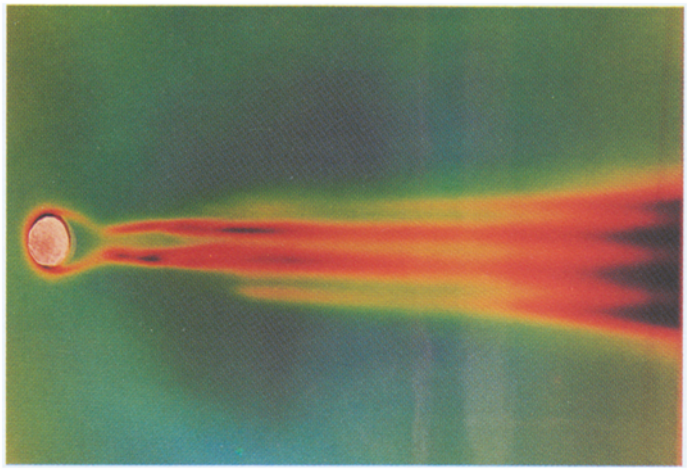

Fig. 4. Liquid crystal flow visualization around and behind a circular cylinder at $L=1.2$ m with $H=1.0$ mm, $h=2.6$, $D_r=28$ mm and $U_\infty=5.0$ m/s

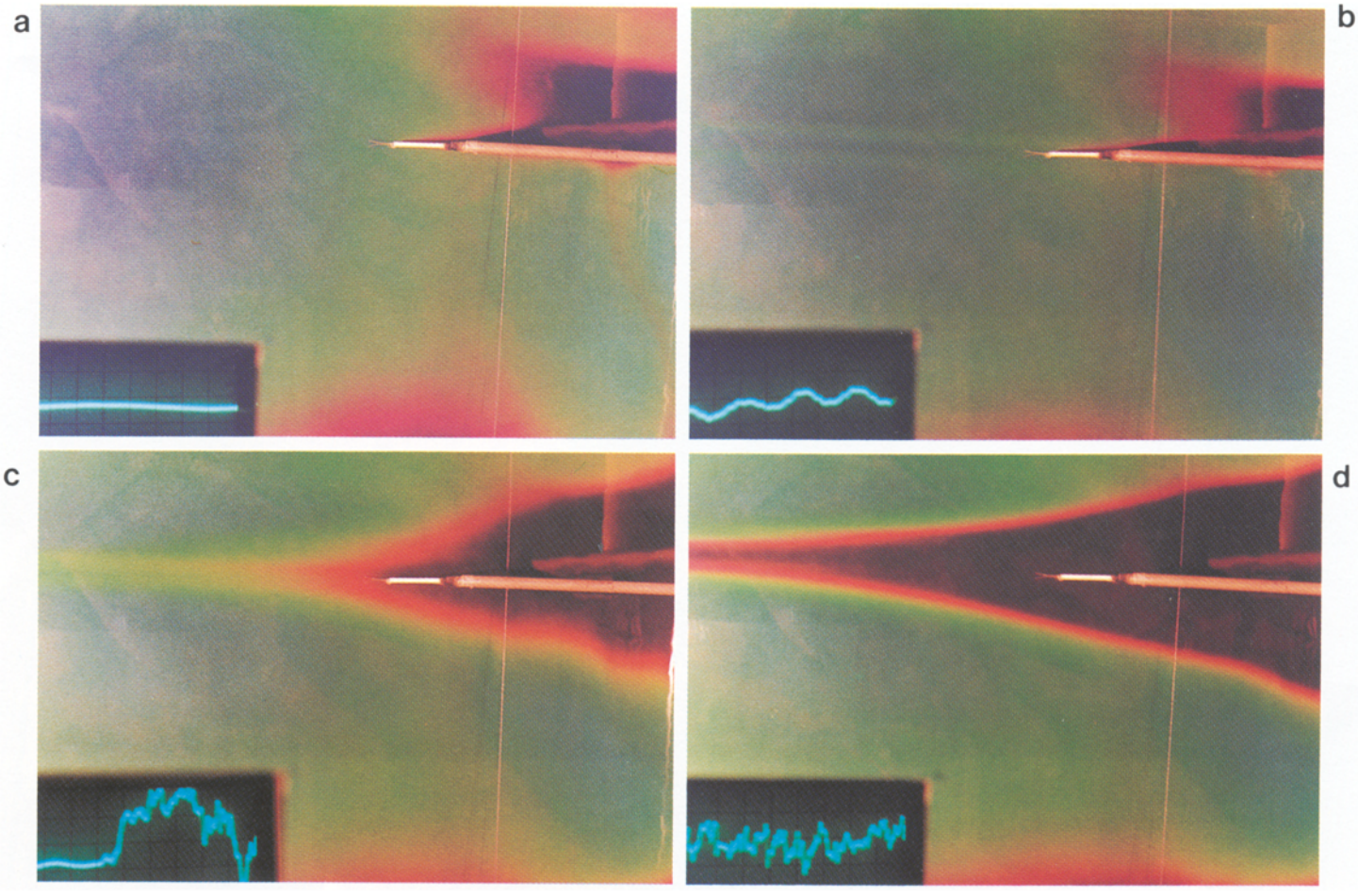

Fig. 5a–d. A comparison of the steady liquid crystal patterns with the hot-wire signals. The experimental conditions for all four photographs are $U_\infty=13$ m/s, $H=0.3$ mm, $D_r=28$ mm, $f=97$ Hz and $Re_L=4.45\cdot10^5$. **a** without excitation, **b** with low excitation level, **c** with medium excitation level, **d** with higher excitation level

was located at $Re_x=0.86\times10^6$. The Reynolds number based on the thickness of the roughness (0.055 mm) and the free stream velocity was 26 and $h=0.24$. The phase averaged wave form of the linearized hot-wire signals (Fig. 6) showed that for cases (a) and (b) the flow was devoid of disturbances even with the tape in place. The intensity of the *T–S* waves for flow (c) was still very weak, which indicated that the receptivity of the flow to the acoustic disturbance was small without the roughness. This weak response may have been due to the leading edge receptivity. The strong response of the flow with the roughness in place (i.e. condition d) shows that the acoustic long wave had been converted into the vorticity short wave through the

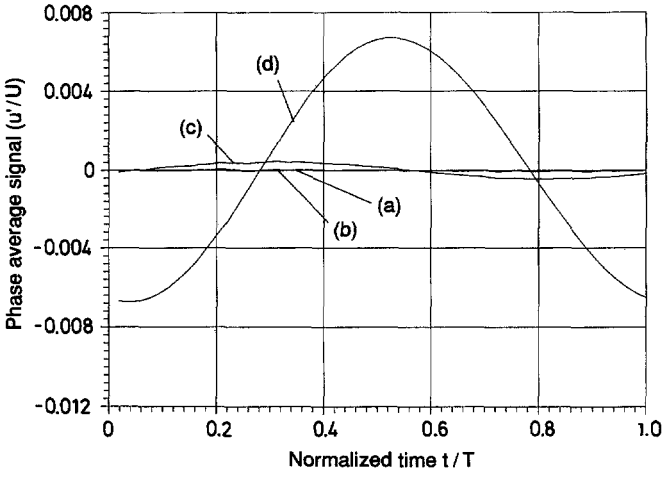

Fig. 6. The phase averaged velocity signals for conditions (*a*) through (*d*) in the text. For all four flows, the experimental parameters are $L=0.59$ m, $U_\infty=7.0$ m/s, $x_m=1.8$ m, $f=38$ Hz, $W=19$ mm, $H=0.055$ mm ($h=0.24$) and SPL = 99 dB

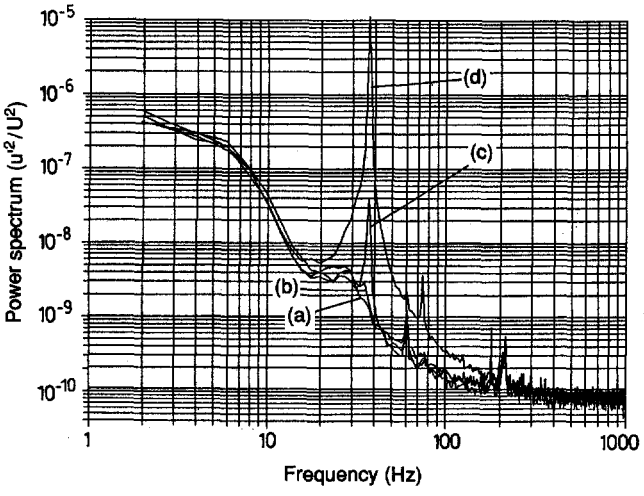

Fig. 7. The spectra corresponding to the flow conditions in Fig. 6

medium of the surface inhomogeneity. The corresponding spectra in Fig. 7 support this conclusion. These figures were taken with a two-dimensional roughness. The results on the centerline behind the three-dimensional roughnesses were similar; i.e. only minute signals were observed without the roughness element.

3.2
Influences of the basic parameters

3.2.1
Incident angle of the acoustic waves

Many of the previous investigations have introduced the acoustical waves far upstream so that their propagation direction was approximately the same as the freestream velocity. In the present study, a more local acoustical source was used and hence the angle of incidence, θ_{ac} in Fig. 2, is an important parameter of the experiment. The pole angle indicated in the figure was defined as having a negative value in accordance with the theory of Choudhari and Kerschen 1990 which is summarized in the Appendix.

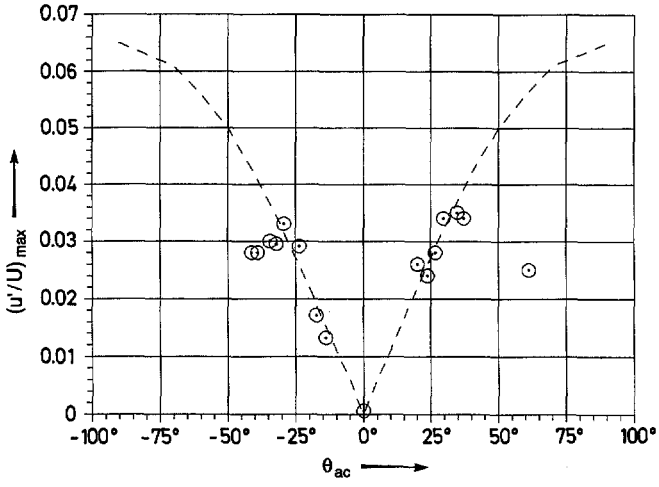

Fig. 8. Influence of the incidence angle of the acoustic was for $L=0.635$ m, $x_m=1.2$ m, $U_\infty=13$ m/s, $f=80$ Hz and $H=0.225$ mm ($h=1.37$)

To investigate the influence of the orientation of the acoustic wave, the streamwise location of the loud speakers was varied but the orientation of the speakers was always perpendicular to the opposing wall. The free stream velocity, the location and height of the roughness and of the hot wire position were all kept constant. The sound pressure level at the tape location was kept at 97 db throughout the test. The results are shown in Fig. 8. The data for $-30^\circ<\theta_{ac}<30^\circ$ are in good agreement with the linear theory (dashed line) given by Choudhari and Kerschen 1990, i.e. the velocity perturbation varies as $\sin\theta_{ac}$ as expressed by the coupling coefficient C(1) in equation (D) from the appendix. The main reason for the departure from the theory at greater angles of incidence was believed to be due to the reflection of the acoustic wave from the tunnel walls. The angle of incidence was fixed at 28 degrees throughout the remaining experiments.

3.2.2
Frequency dependency

For laminar-turbulence transition, the frequency of the disturbance is one of the most important parameters. However since receptivity is an entirely different aspect of transition, it is not clear that frequency influences receptivity in the same manner as it influences instability. Nevertheless, since the long wave acoustical waves are converted into short wave length vortical disturbances by the presence of the roughness, the frequency range should be similar to that of the *T–S* waves. Thus this study concentrated on those frequencies which were amplified downstream according to the *T–S* instability.

Figure 9 shows the power spectra downstream of a 0.055 mm high two-dimensional roughness element for five different excitation frequencies. The maximum spectral peak occurred when the excitation frequency matched the most amplified *T–S* frequency at 32 Hz. This suggests that the *T–S* wave is the

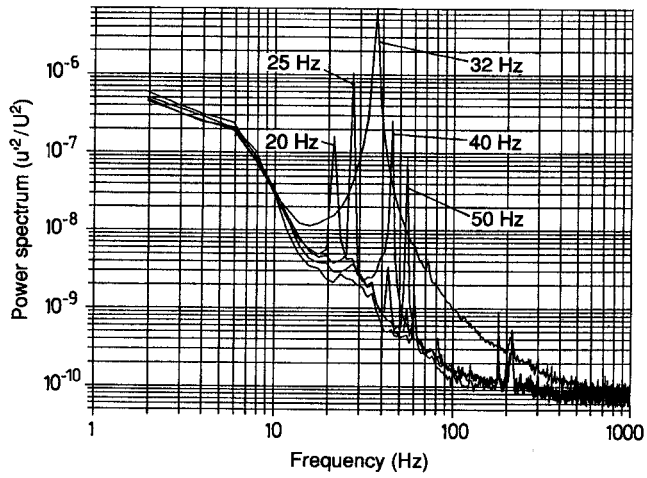

Fig. 9. Frequency response of the flow for $L=0.59$ m, $x_m=1.8$ m, $U_\infty=7.0$ m/s, $W=19$ mm, $H=0.055$ mm ($h=0.23$) and SPL = 99 dB. The five forcing frequencies are given in the figure

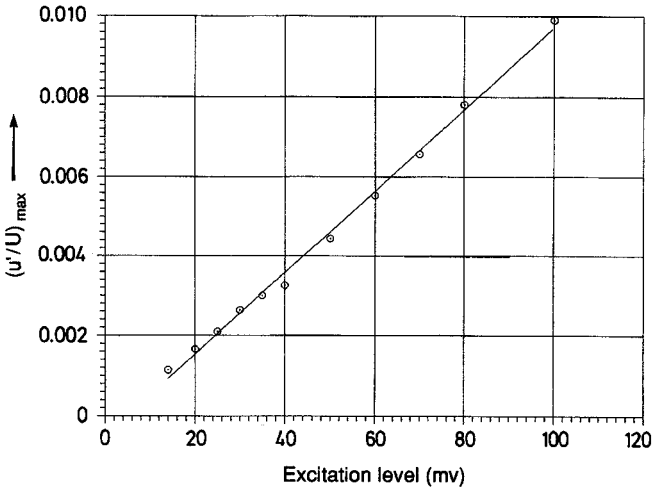

Fig. 10. Influence of the excitation amplitude on the velocity disturbance measured at 2.0 m. The other parameters are $L=0.80$ m, $W=19$ mm, $U_\infty=7.0$ m/s, $f=38$ Hz and $H=0.055$ mm ($h=0.21$)

dominant wave if the fetch distance is long enough that sufficient amplification occurs. However, this may not be true in general since the disturbances undergo different amplification rates as they propagate to the location of the hot-wire probe.

3.2.3
Excitation amplitude

The effect of the excitation amplitude on the flow response is shown in Fig. 10. The excitation levels were measured by a quarter inch diameter microphone at the reference location. The maximum and minimum voltages on the abscissa correspond to a sound pressure level of 100 dB and 82 dB respectively. The velocity amplitude was obtained from the maximum of the phase averaged hot-wire velocity data. The line in Fig. 10 is a least squares fit of a linear curve through the data. As seen, the relationship between the two was linear for these levels of excitation. This agrees with Choudhari

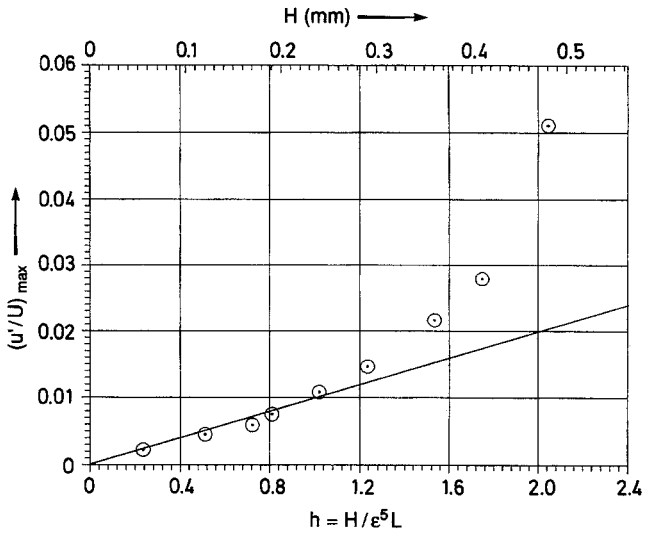

Fig. 11. Effect of roughness height on the receptivity for the conditions $L=0.59$ m, $x_m=1.8$ m, $W=19$ mm, $U_\infty=7.0$ m/s and $f=38$ Hz

and Kerschen's 1990 results reproduced as equations (A) and (C) in the Appendix. For the flow parameters and roughness height ($h=0.21$) utilized in Fig. 10, no nonlinear response was obtained at the highest excitation level utilized, i.e. SPL = 100 dB.

3.2.4
Roughness height

The roughness height is an extremely important manufacturing parameter for aircraft surfaces, pipe walls, etc. To investigate this effect, two-dimensional tapes with various thickness were selected as the artificial roughnesses. The amplitudes of the phase averaged velocities are shown in Fig. 11 plotted against the non-dimensional height, $h=H/(\varepsilon^5 L)$. The flow conditions matched those in Fig. 6 and 7. It was clear that there is a region where the receptivity or the coupling coefficient was proportional to the tape thickness for $h \lesssim 1.2$. For larger values of the thickness, nonlinear effects became obvious. The theory derived by Bodonyi et al. 1989 showed that the non-linear effects are important for $h>1$. Their Fig. 10 shows excellent agreement with the present Fig. 11. However, the above does not imply that $h \approx 1.2$ is a necessary criterion for linear receptivity, because nonlinear amplification of the instability waves could have occurred downstream of the roughness before reaching the sensor.

3.3
Other geometrical parameters of the roughnesses

3.3.1
Diameter of the 3-D roughness

Figure 12 shows the influence of the diameter of a circular 3-D roughness on the receptivity. Since the receptivity coefficient ($P_{T-S}/(P_{ac}e^{-iSt})$) was proportional to the excitation level and to the roughness height, the values shown in Fig. 12 are normalized by these two factors. The diameter normalized by the T–S wavelength is given on the abscissa. When other parameters were kept constant, the receptivity coefficient was maximum when the

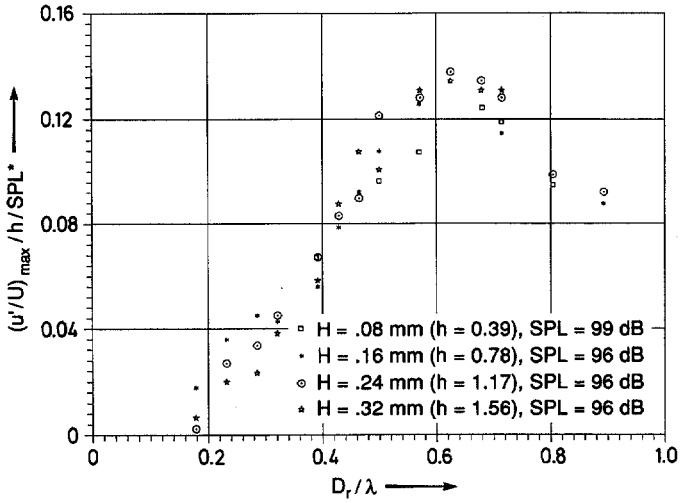

Fig. 12. Influence of the diameter of the roughness at $L=1.15$ m on the receptivity at $x_m=1.8$ m for $U_\infty=13$ m/s and $f=74$ Hz

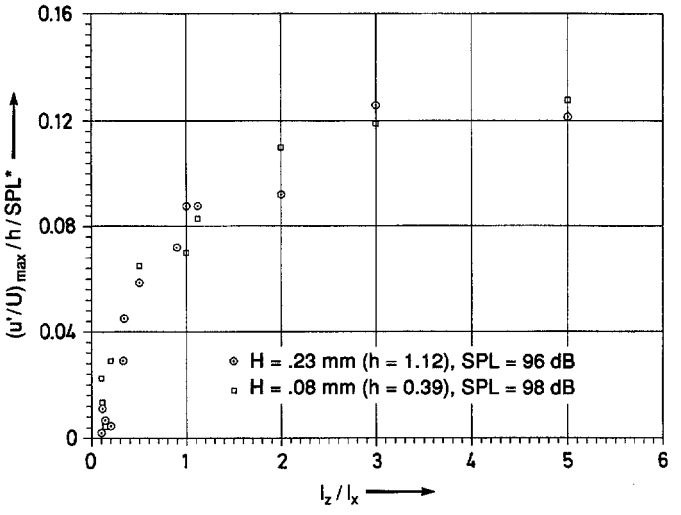

Fig. 13. Effect of varying the aspect ratio of the roughness at $L=1.15$ mm on the velocity disturbance measured at $x_m=1.8$ m, $U_\infty=13$ m/s and $f=74$ Hz

ratio of the diameter to the *T–S* wavelength is roughly 0.6, i.e. slightly more than the half wavelength. These results are almost the same as Choudhari and Kerschen's 1990 predictions found in their Fig. 8. In particular, the maximum receptivity for 3-D roughness elements occurs for diameters of approximately $0.6\,\lambda$ in both the theoretical and experimental cases.

3.3.2
Aspect ratio of the 3-D roughness

Figure 13 shows the influence of the aspect ratio of elliptical 3-D roughnesses on the receptivity coefficient. Two roughness heights were used as indicated in the figure. The area of the roughness, $l_x \cdot l_z$, was held constant at 675 mm^2 with $8.2 < l_z < 58$ mm and $11 < l_x < 82$ mm. The velocity disturbance scale on the ordinate was normalized by the roughness height and by the excitation level. The results agree well with the predictions of Choudhari and Kerschen 1990. For excitation

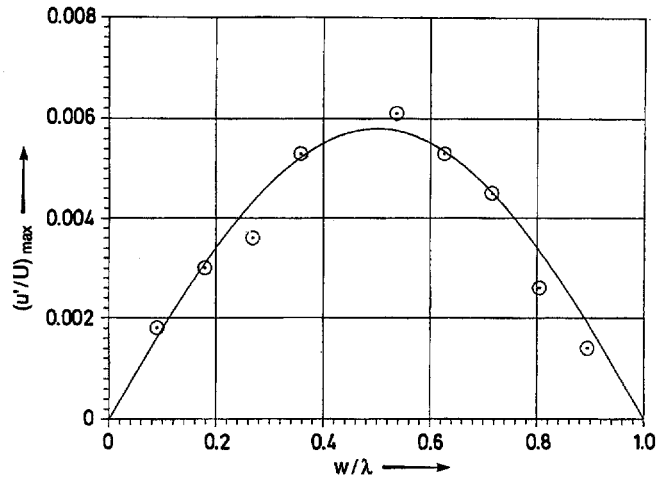

Fig. 14. Influence of the 2-D roughness width on the receptivity for roughnesses at $L=1.15$ m with heights of $H=0.075$ mm ($h=0.37$) measured at $x_m=1.8$ m with $U_\infty=13$ m/s, $f=74$ Hz and SPL = 99 dB

frequencies corresponding to the most amplified *T–S* waves, the receptivity increased with increasing aspect ratio until it reached an asymptotic value corresponding to the 2-D roughness.

3.3.3
Tape width of the 2-D roughness

Goldstein 1985 shows that linear theory predicts that the receptivity coefficient should reach its maximum when the roughness width is equal to half the wavelength of the most amplified *T–S* wave. This prediction was tested and the results are shown in Fig. 14 plotted versus W/λ. The maximum value at $W/\lambda \approx \frac{1}{2}$ indicates that the effect of the two-dimensional roughness' width on the receptivity coefficient is indeed given well by the linear theory. In addition, when equation B in the appendix is integrated for the case of a strip roughness, the receptivity coefficient has a $\sin(\pi \cdot W/\lambda)$ dependence. This functional dependency is displayed in Fig. 14 with the amplitude adjusted to give a best fit.

At first sight, the results in Fig. 14 seems contrary to Saric, Hoos and Kohama's 1990 results in which they state that the "width of the roughness element is not a dominating factor in the receptivity process ..." However in their experiments, the frequency, i.e. wavelength, of the perturbation was varied and the width of the roughness was held constant. Although this makes the experiment easier to perform, it has the disadvantage that the amplification is different for each wavelength. In Fig. 14 the width of the roughness element was varied but the frequency and wavelength were held constant. Thus in the present experiments, the amplification due to the instability was held constant throughout the experiment. This would seem to account for the differences between these two sets of experiments.

3.3.4
Sweepback angle of the 2-D roughness

To determine whether a sweepback roughness could generate an inclined wave with the same azimuthal angle, an inclined 2-D tape was fixed on the test surface with various sweepback angles. Two single hot-wire probes with a spanwise separation of 40 mm were located at the same distance from the leading edge. The

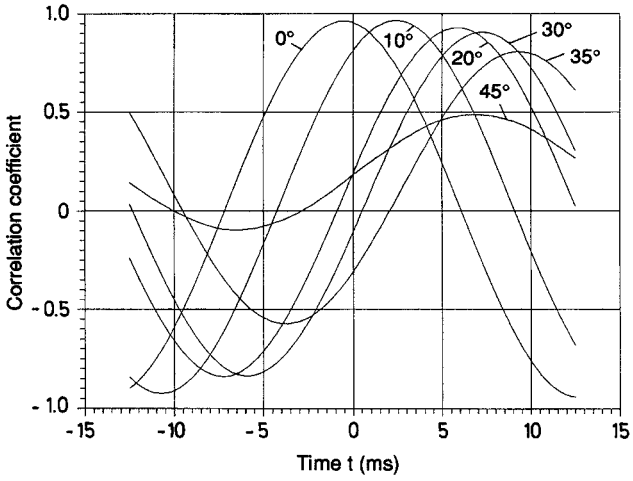

Fig. 15. Cross correlation of two velocity signals with 40 mm spanwise separation behind the oblique roughness. The experimental conditions are $L=0.59$ m, $x_m=1.6$ m, $U_\infty=7.0$ m/s, $H=0.12$ mm ($h=0.51$), $f=38$ Hz and SPL = 97 dB

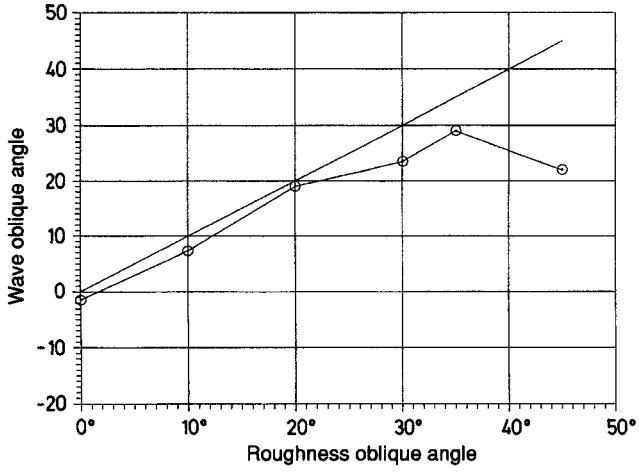

Fig. 16. The computed wave angles behind an oblique roughness element. The experimental conditions were the same as in Fig. 15

correlation coefficients between the two signals were measured with a time delay, τ, and are shown in Fig. 15. As the sweep angle increases, the correlation maximum increases monotonically until approximately 35°.

The effect of the swept roughness in generating a swept wave can best be seen by converting the time lag into distance, Δx, by means of Taylor's hypothesis. The wave angle is then given by $\tan^{-1}(\Delta x/\Delta z)$ where Δz is the distance between the two probes. Figure 16 shows that the waves behind the tape were almost parallel to the tape when the sweepback angle was less than 20 degrees.

Phase averaged amplitudes behind the inclined tape were also processed and shown in Fig. 17. The results could not be simply expressed as being proportional to $\cos\phi_{ac}$ (see equation B in the appendix) because a change of the roughness sweepback angle varied both the effective incidental angle of the acoustic wave at different spanwise location of the tape and also varied

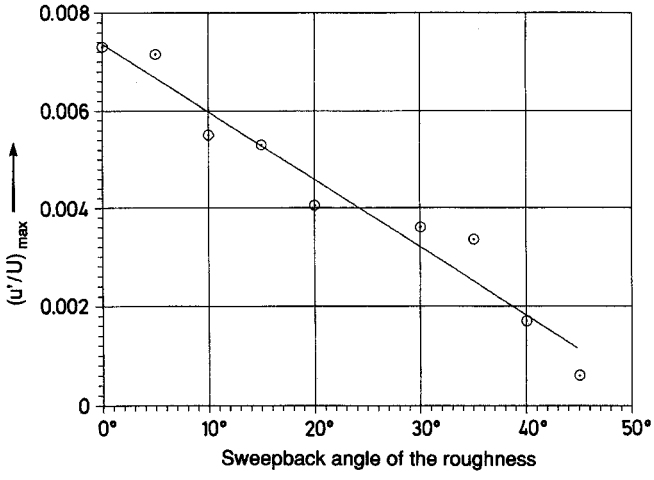

Fig. 17. Influence of oblique angle of the roughness on the receptivity. The experimental conditions were the same as in Fig. 15. The line is a best fit linear curve

the effective streamwise location of the tapes. However, the qualitative tendency was still the same as the theory, i.e. the greater the oblique angle, the weaker the receptivity.

4 Conclusions

The liquid crystal visualization and the hot-wire data have both shown that the receptivity of the laminar boundary layer to acoustic waves is caused by the interaction of the acoustic field with the surface roughness rather than by the acoustic disturbances alone. Both the two- and three-dimensional roughnesses yielded a linear response for small roughness heights and excitation amplitudes. Since the roughness elements were always within the unstable region of the laminar boundary layer, the most predominate response corresponded to the most amplified Tollmien–Schlichting wave predicted by linear stability theory. As the width and/or the diameter of the roughness changed, the maximum response was obtained for waves with approximately half the wavelength of the *T–S* wave. In the two-dimensional case, the onset of nonlinearity as the height increased agreed well with the predictions of Bodonyi et al. 1989. The general results, especially the three-dimensional ones, confirm the predictions of Choudhari and Kerschen 1990.

Appendix: Theoretical background

As is well known, acoustic waves at a fixed frequency are much longer than the wavelengths of the instability vorticity waves. Furthermore, the former propagate at a much higher speed than the latter. Acoustical receptivity implies that some streamwise non-uniformity must be present to convert the acoustic waves to vortical waves. Thus an ideal laminar boundary layer on a perfectly smooth infinite flat plate with an absolutely uniform streamwise mean velocity will not accept any acoustic disturbances. Impinging acoustic waves can be converted into vorticity waves if and only if there is considerable variation of streamwise mean velocity which can result from a leading edge, pressure gradient, surface roughness, etc.

According to Choudhari and Kerschen 1990, the unsteady pressure caused by the instability wave corresponds to an infinite sum of modes:

$$P_{T-S} = P_{ac} e^{-iSt} \sum_{-\infty}^{\infty} C_n e^{i(\kappa_n X - l_n Z)} \tag{A}$$

The sequence of coupling coefficients C_n is given by:

$$C_n = 2\sqrt{\frac{2\pi}{d_z}} M_\infty \frac{H_w}{\varepsilon^5 L} [\sin\theta_{ac} \cos(\phi_n - \phi_{ac})] \times (\cos\phi_n)\, \lambda \kappa_n F_n(-\kappa_n)\, \Lambda\left(\frac{S}{\sqrt{\lambda^3 \cos\phi_n}}\right) \Xi_n \tag{B}$$

where:

P_{T-S} the instability wave contribution to the unsteady pressure
P_{ac} the input acoustic pressure
d_z fundamental wave number of the roughness in the Z direction.
M_∞ Mach number of the free stream
H_w roughness height
$\varepsilon = (U_\infty L/\nu)^{-1/8}$
L position of roughness in X direction
θ_{ac} angle of incident acoustic wave (o for normal to the wall)
ϕ_n azimuthal angle of wave number vector of the roughness (o for streamwise direction)
ϕ_{ac} azimuthal angle of propagation of the acoustic wave
$\lambda = (dU/dy)_{y=0}$ nondimensional shear stress at the wall
κ_n streamwise wave number of the roughness
l_n spanwise wave number of the roughness
$F_n(-\kappa_n)$ Fourier transform of the spatial distribution of the wall inhomogeneity
Λ intrinsic efficiency functions for various receptivity mechanisms, which depend on the equivalent 2-D frequency

$$S_n = S/\sqrt{\cos\phi_n}$$

$S = \varepsilon^2 \omega L/U_\infty$ nondimensional acoustic frequency
Ξ_n is defined as:

$$\Xi_n = \frac{1}{1 + \dfrac{3S_n \partial \Delta_{(2-D)}/\partial S}{4\eta_n \partial \Delta_{(2-D)}/\partial \eta}}$$

where $\Delta_{(2-D)}$ corresponds to an equivalent 2-D form of the dispersion relation given by

$$\Delta_{(2-D)}(\kappa(\cos\phi)^{-3/4}; S(\cos\phi^{-1/2})) = \Delta_n(\kappa; S) = 0$$

and $\Delta_n(\kappa; S)$ corresponds to a 3-D dispersion relation as described in Choudhari and Kerschen 1990 as

$$\Delta_n(\kappa; S) \equiv \int_\eta^\infty A_i(\eta)\, d\eta - i \frac{\kappa}{\sqrt{\kappa^2 + l_n^2}} \frac{\eta^2 \lambda^3}{S^2} A_i'(\eta) = 0$$

$$\eta = -iS/(-i\kappa\lambda)^{2/3}$$

For a single isolated 3-D roughness, the coupling coefficient function can be obtained by allowing d_z to approach infinity and can be expressed as follows:

$$P_{T-S} = P_{ac} e^{-iSt} \int_{-\infty}^{\infty} C(l)\, e^{Xh(l)}\, dl \tag{C}$$

with

$$C(l) = \sqrt{\frac{2}{\pi}} M_\infty \frac{H_w}{\varepsilon^5 L} [\sin\theta_{ac} \cos(\phi - \phi_{ac})] (\cos\phi) \times \lambda \kappa(l) F(-\kappa(l), l)\, \Lambda\left(\frac{S}{\sqrt{\lambda^3 \cos\phi}}\right) \Xi \tag{D}$$

where $C(l)$ is the coupling coefficient function and the subscript n on ϕ, κ and Ξ has been dropped for these quantities are considered to be functions of l.

$h = i(\kappa - l \cdot \tan\phi')$ and $\tan\phi' = Z/X$

$\kappa(l)$ is the streamwise wave number of the roughness as a function of l, $F(-\kappa(l), l)$ is the two dimensional Fourier transform of the appropriately normalized spatial distribution of the wall inhomogeneity.

Equations (A), (B), (C) and (D) provide the influences of various parameters as studied in the main part of this paper.

References

Blackwelder RF; Haritonidis JH (1983) Scaling of the Bursting Frequency in Turbulent Boundary layers. J Fluid Mech 132: 87

Bodonyi RJ; Welch WJC; Duck PW; Tadjfar M (1989) A numerical study of the interaction between unsteady freestream disturbance and localized variations in surface geometry. J Fluid Mech 209: 285–308

Choudhari M; Kerschen EJ (1990) Instability wave patterns generated by interaction of sound wave with three-dimensional wall suction or roughness. AIAA-90-0119

Goldstein ME (1983) The evolution of Tollmien–Schlichting waves near a leading edge. J Fluid Mech 127: 59–81

Goldstein ME (1985) Scattering of acoustic waves into Tollmien–Schlichting waves by small streamwise variations in surface geometry. J Fluid Mech 154: 509–529

Kerschen EJ; Choudhari M; Heinrich RA (1989) Generation of boundary layer instability waves by acoustic and vortical free stream disturbances. Proceedings IUTAM 3rd. Symposium on Laminar-Turbulent Transition, Toulouse

Kerschen E (1989) Boundary layer receptivity. AIAA-89-1109

Kerschen EJ (1990) Boundary layer receptivity theory. Appl Mech Rev 43 No. 5, Part 2

Nishioka M; Morkovin MV (1986) Boundary layer receptivity to unsteady pressure gradients: experiments and overview. J Fluid Mech 171: 219–261

Saric WS, Hoos JA; Radeztsky RH (1991) Boundary layer receptivity of sound with roughness. Proc. Symposium on Boundary Layer Stability and Transition to Turbulence, Portland

Saric WS; Hoos JA; Kohama Y (1990) Boundary layer receptivity Part 1, Freestream sound and 2-D roughness strips. CEAS-CR-R-90191